Journal of
*Composites Science*

MDPI

*Article*

# Tailored Compositions of Ni-Ti-Sn Nanopowders Deposited on Polymer Fiber Optics Through Flash Evaporation

**Elango Natarajan [1,*], Anil Chouhan [1], Santheraleka Ramanathan [1], Kalaimani Markandan [1], Santhosh Mozhuguan Sekar [1], Chun Kit Ang [1], Nagarajan Deivanayagampillai [2] and Gérald Franz [3,*]**

[1] Faculty of Engineering, Technology and Built Environment, UCSI University, Kuala Lumpur 56000, Malaysia; santheraleka@ucsiuniversity.edu.my (S.R.); kalaimani@ucsiuniversity.edu.my (K.M.); santhosh@ucsiuniversity.edu.my (S.M.S.)
[2] Department of Mathematics, Rajalakshmi Institute of Technology, Chennai 600124, India; dnrmsu2002@yahoo.com
[3] Laboratoire des Technologies Innovantes, UR UPJV 3899, Avenue des Facultés, Le Bailly, 80025 Amiens, France
* Correspondence: elango@ucsiuniversity.edu.my (E.N.); gerald.franz@u-picardie.fr (G.F.)

**Abstract:** Fiber coatings protect the glass surface of fiber from extrinsic environmental factors. The coating of shape memory alloy over fiber is useful in sensor fabrication where the state of deformation is affected by the phase transformation of the coated material. In addition, coated plastic fibers can be used in elevated temperature environments. To this end, the present research aims to investigate the effect of the Ni-Ti-Sn composite coating over the fiber. Homogeneous particle distribution, agglomeration, porosity and the ability to obtain uniform coating thickness have been general concerns in fiber coatings. Hence, the present study comprehensively investigated the mechanical and thermal behavior as well as morphological properties of Ni-Ti-Sn nanopowders deposited on polymer fiber optics. Five sets of polyamide-coated samples with different Ni-Ti-Sn proportions were fabricated and characterized. Morphological studies confirmed that an even coating thickness enhanced the mechanical integrity and optical performance. The optimum composition demonstrated superior tensile strength of 29.5 MPa and a 25% increase in elongation compared to the uncoated sample. The Ni-Ti-Sn alloy composition investigated in the present study is promising for industrial applications where thermal stability and mechanical performance are warranted.

**Keywords:** polymer fiber; nanopowder coating; Ni-Ti-Sn alloy; thermal analysis; product innovation



**Citation:** Natarajan, E.; Chouhan, A.; Ramanathan, S.; Markandan, K.; Mozhuguan Sekar, S.; Ang, C.K.; Deivanayagampillai, N.; Franz, G. Tailored Compositions of Ni-Ti-Sn Nanopowders Deposited on Polymer Fiber Optics Through Flash Evaporation. *J. Compos. Sci.* **2024**, *8*, 526. https://doi.org/10.3390/jcs8120526

Academic Editors: Xiangfa Wu and Oksana Zholobko

Received: 16 October 2024
Revised: 29 November 2024
Accepted: 6 December 2024
Published: 13 December 2024



## 1. Introduction

Fiber optics are an essential part of the telecommunication and networking industry due to its lightweight nature, accessibility, and effective data transmission [1,2]. It has been observed that the development of optical fibers has played a significant role in the revolutionizing procedure for data communication systems by enabling faster transmission over longer distances [3]. Coatings on optical fibers significantly improve mechanical, thermal, and optical properties that have enhanced the strength of such fibers operating under various environmental conditions. The term "fiber coating" refers to a protective layer applied to the optical fiber and is usually made from materials such as acrylate, polyimide, or silicone that protect the fibers from physical damage, environmental effects, and mechanical stress, which would lead to signal deterioration or even fiber failure [4–6]. These coatings have particular importance for the reliability and efficiency of fiber optic communication systems underlying contemporary digital infrastructure in telecommunications, data transmission, and networking. While impressive progress has occurred, the field of fiber optics still faces challenges such as mechanical degradation, vulnerability to environmental elements, and signal loss, further emphasizing continuous research into fiber coatings for the sake of performance and durability in optical fibers. To date, extensive

studies have been performed and reported in the open literature with a range of fiber coating materials based on polymers, metals, and/or ceramics [7,8]. A polymer-based coating has been extensively used because of its intrinsic flexibility, ease of application, and protection provided to the fibers against external threats such as moisture and chemical attack [9]. These coatings represented an important advance in the 1970s, which coincided with the commercialization of polymer-coated optical fibers, supposing their extensive application in terrestrial and underwater fiber optic communication networks. With the invention of different polymer materials like silicone and acrylate, it protected against their mechanical damage, water ingression, and deterioration that would result from environmental exposure. However, while these polymer-derived coatings have provided aspects of protection, more advanced coating materials must be employed in aggressive environments, such as at high temperatures and in corrosive media.

Subsequent advances in fiber coating technology encouraged further studies into metallic and alloy coatings, offering even greater mechanical durability, corrosion resistance, and thermal stability. Research into metal coatings such as Ni, Ti, and Sn has been carried out to establish their potential in improving the performance of optical fibers, especially for industrial and high-performance applications [10,11]. Nickel contributes excellent electromagnetic interference shielding, titanium provides temperature stability, and tin contributes to electrical conductivity. The resulting properties make the metal coatings more desirable in extreme application conditions such as those encountered in aerospace, automotive, and biomedical sectors [12,13]. Despite the many benefits of such metal coatings, how to combine the metals in optimal alloys remains one of the most active gaps in knowledge relating to fiber coatings. Traditional deposition processes have also faced challenges in achieving uniform coatings with precise thickness control, which is critical to the performance and reliability of fiber optic systems in the industry [14,15]. Recent studies have shown promise in the use of alloy coatings to enhance fiber performance, particularly the Ni-Ti-Sn alloy. The Ni-Ti-Sn alloys are a unique combination of mechanical, thermal, and corrosion-resistant properties that make them particularly suitable for high-performance fiber optics. The addition of nickel and titanium in the alloy significantly increases its strength and durability, whereas the addition of tin enhances both the electrical conductivity and thermal stability of the alloy [16–18]. Flash evaporation, which is known for producing high-quality and very uniform coatings with much careful control over thickness and composition, has emerged as an exceptionally effective method for applying Ni-Ti-Sn alloy coatings. Flash evaporation allows for the controlled deposition of thin alloy films onto the fibers' surface, thus ensuring a uniformly distributed coating with enhancement in mechanical integrity [19,20]. The application of a Ni-Ti-Sn coating on fibers remains rather under-investigated in the literature until now; thus, this area opens up vast opportunities for further research related to the effectiveness of such a coating in enhancing fiber performance against harsh environmental conditions [21].

Despite the promising results, there is still a gap in the research literature regarding the optimization of Ni-Ti-Sn alloy coatings for specific industrial applications [22]. For instance, polyamide is one of the common materials used in belt drive systems and optical cables. The critical concern with the use of this plastic material under high stress is its tendency to break without warning, which could potentially lead to industrial failure. While previous studies have shown that metal coatings have the potential to enhance the durability and performance of optical fibers [23], the unique combination of nickel, titanium, and tin has not been fully explored on polyamide optical fibers. Addressing the aforementioned research gap will improve the performance and reliability of polyamide fiber in various industrial applications. To this end, this paper examines the mechanical and thermal behavior of Ni-Ti-Sn polyamide-coated samples. Findings obtained from the present study ascertain potential applications of Ni-Ti-Sn polyamide-coated samples in structural health monitoring and biomedical devices.

## 2. Materials and Methods

### 2.1. Material

The principal single-mode optical fiber, coated with polyamide, was procured from a local store. It had a 1 mm diameter, 0.5 mm core diameter and length of 200 mm. Ni, Ti, and Sn(Tin) nanopowder was acquired from SRL chemicals, India.

### 2.2. Fabrication of Ni-Ti-Sn Coating on Fiber

The flash evaporation method was used to deposit a Ni-Ti-Sn thin-film composite coating onto a plastic optical fiber cable. Flash evaporation is an excellent technique to produce thin and uniform coatings that are essential in optics, electronics, and many other industrial applications. In fact, the purity and control produced via this technique on its films make it irreplaceable in the field of materials science and engineering. In flash evaporation, the source material in the form of a fine wire or powder will be continually fed into the hot evaporation chamber [24,25]. The polyamide–host material was mounted onto an in situ rotatable fixture that allows the uniform deposition of a Ni-Ti-Sn coating on its entire circumference. Prior to coating, the host material was pre-strained to 5% by mechanical loading, and the experimental setup was cleaned with acetone. The adjustment in rotational speed within the system assisted in varying the thickness of the coating [26,27].

The process was carried out under a high-vacuum environment at $5 \times 10^{-5}$ Mbar pressure and at room temperature (20 °C). A detailed scheme of the flash evaporation process is shown in Figure 1a. Firstly, an appropriate volume percentage of Ni-Ti powders and Sn powders was mixed for 30 min. After the homogeneous mixing of powders, the mixture was placed into a tungsten boat within the evaporation chamber. A current of 120 A was applied to evaporate the Ni-Ti-Sn powder from the tungsten boat. At the same time, the rotational speed of the in situ fixture was adjusted between 100 and 300 rpm to evenly coat the composite material over the entire circumference of the host optical fiber. The coating duration takes 30 min inclusive of a 20-min cooling period. The average coating thickness of the samples was about 0.50 µm, and it was measured using microscopic images. Table 1 summarizes the developed samples and their compositions, where the composition of Ti is the same for all sets and the amounts of Ni and Sn were manipulated to evaluate the efficiency of the coated polyamide optical fiber material.

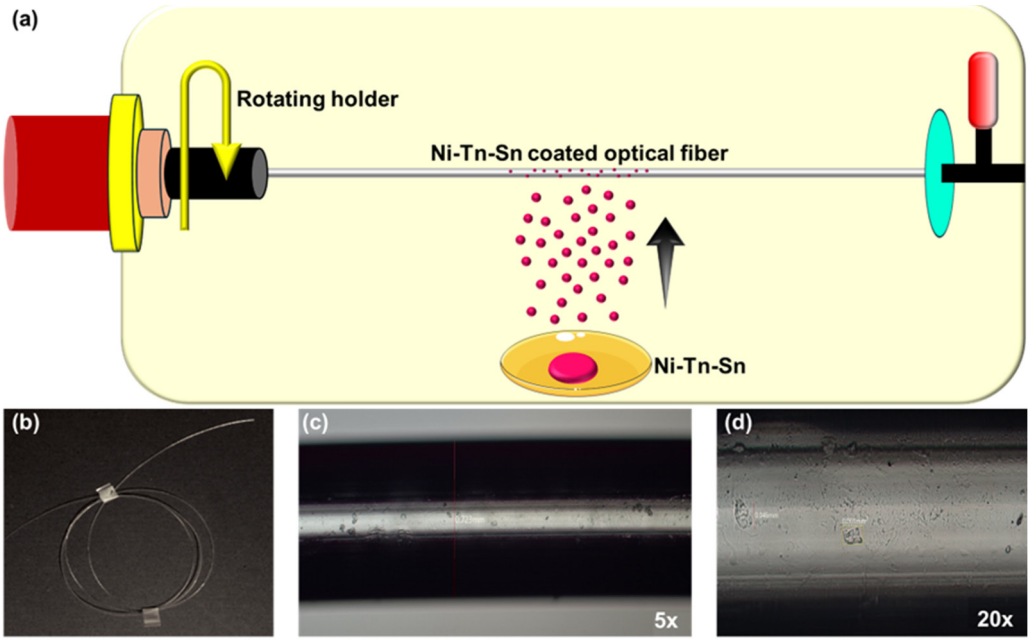


**Figure 1.** (**a**) Schematic illustration of flash evaporation process of coating optical fiber with Ni-Ti-Sn nanopowders. (**b**) Digital image of optical fiber used in the study. HPM images of uncoated fiber at (**c**) 5× and (**d**) 20× magnification.

**Table 1.** Experimental compositions of fiber coating using Ni-Ti-Sn.

| Sample | Ni (%) | Ti (%) | Sn (%) |
|---|---|---|---|
| Set 1 | 47.8 | 50.2 | 2.0 |
| Set 2 | 48.3 | 50.2 | 1.5 |
| Set 3 | 48.1 | 50.2 | 1.7 |
| Set 4 | 48.5 | 50.2 | 1.3 |
| Set 5 | 48.8 | 50.2 | 1.0 |

### *2.3. Characterization of Coated Samples*

A high-power microscope was used to study the morphology of optical fibers coated with different quantities of Ni-Ti-Sn elements. This microscopic analysis allowed for observing the surface texture, homogeneity of the coating, and any possible defects that may affect the performance of the fibers. Surface analysis with better resolution was conducted using a field emission scanning electron microscope (SEM), model JSM-7600F (JEOL Inc., Tokyo, Japan) with an accelerating voltage of 2–5 kV. The FESEM images before and after the fracture of Ni-Ti-Sn-coated fibers were carried out to study the coating smoothness, distribution of particles, and surface characteristics, which would give a complete microstructural view for the coated fibers. In addition to the morphological analysis, the samples were analyzed using Fourier Transform Infrared (FTIR) spectroscopy to determine the intensity of Ni-Tn-Sn in each of the coated fibers. The coated fibers were placed on a KBr pellet and scanned from 4000 to 500 $cm^{-1}$.

Tensile testing was performed according to the ASTM D3822 standard to investigate the mechanical performance of the coated samples in terms of strength, elasticity, and elongation using an Instron universal tensile testing machine (6800 Series, Norwood, MA, USA). The testing provided valuable information on the mechanical stability of the coated fibers and its efficacy under stress conditions to be estimated.

Thermogravimetric analysis (TGA) was performed to investigate the change in mass in the coated samples with rising temperature, which provided useful information on the thermal stability of the coated samples. This test was performed using a Perkin Elmer TGA 4000 equipped with Pyris software. Tests were conducted up to an upper temperature limit of 600 °C, and the resultant data were analyzed to evaluate the thermal degradation properties of the coated and uncoated fiber samples.

Thermal behavior and the determination of appropriate heat treatment temperatures of coatings were evaluated by differential thermal analysis (DTA) using the STA-6000 device. Thermal analysis in nanopowder-coated fiber was performed at a heating rate of 10 °C/min. $\alpha$-alumina was used as the reference material, and the increasing rate was set at 10° C/min. The appropriate heat treatment, to achieve the desired crystalline phase in the coatings, was performed for 2 h in an electric furnace at the maximum crystallization temperature determined by DTA.

## 3. Results and Discussion

### *3.1. Morphology Studies*

Coating surfaces were examined at several levels of magnification to evaluate characteristics such as the thickness and evenness of the coating, its ability to adhere, and the presence of any flaws such as cracks, cavities, or inclusions. A HPM (high-pressure microscope) was used to acquire images of regions of interest, while Olympus imaging software was used for in-depth analysis, such as measuring characteristics and creating thorough reports. Figure 1b depicts the digital image of uncoated optical fibers used in the study. The microscopic view of uncoated fiber under HPM is shown in Figure 1c,d at 5× and 20× magnification, respectively. The uncoated fibers have a range of surface flaws, such as noticeable scratches, debris, and irregularities, with measurements indicating deficiencies of 0.022 mm, 0.046 mm, and 0.070 mm. These flaws indicate a deficiency in the fiber-protective layer, which might result in the degradation and malfunction of the object.

Figure 2 shows the HPM images of Ni-Ti-Sn-coated fibers at three different magnifications with varying compositions. The row of a, b, and c in Figure 2 denotes the HPM images captured at 5×, 20×, and 50× magnification. Fibers coated with the Set 1 (Figure 2—Set1) composition showed an even surface and fewer imperfections, suggesting that the coating has enhanced the overall quality of the surface where it measures 0.111 mm and 0.047 mm in the coated samples, indicating a significant decrease in both the size and occurrence of surface irregularities compared to the untreated samples. The comparison highlights the efficacy of the Set 1 coating in improving surface quality, offering superior protection, and perhaps prolonging the lifetime and dependability of the material. The layers of Ni-Ti-Sn-coated fibers are clearly shown in Figure 2-Set 1b, which further affirms the even coating of the nanopowders. Figure 2-Set1c depicts the magnified view of Ni-Ti-Sn layers coated on optical fiber. The Set 2 optical images shown in Figure 2-Set2a-c exhibit pronounced surface features, including significant ridges and valleys with notable measurements of 0.056 mm, 0.03 mm, and 0.06 mm, which suggest a coarser and more irregular surface texture. These images indicate that Set 2 may have issues with surface flatness and uniformity. In contrast, Figure 2-Set 3a-c images show a surface that is more uniform and smoother. The measurements, which encompass 0.175 mm and smaller defect areas such as 0.007 mm and 0.01 mm, suggest a superior surface finish with fewer and smaller defects. This comparison emphasizes that Set 3 coating has a superior performance in delivering a surface that is free of defects and more uniform, which can considerably improve the material's functional properties and durability. The measurements for the Set 4 composition coated on the fiber were 0.026 mm, 0.09 mm, and 0.03 mm, revealing a relatively rough surface with visible imperfections such as debris and surface flaws. This suggests that the Set 4 coating process faces challenges in achieving a completely smooth and uniform surface. Set 5 samples had dimensions of 0.098 $mm^2$, 0.037 mm, and 0.025 mm, respectively. In both cases, the surfaces showed minor imperfections characterized by rough and irregular coating coverage; there is, however, a slight diminution in size and the numbers of imperfections compared to the previous Set 4. By comparison, Set 5 allows a close-to-better quality of the surface in Figure 2-Set5-a-c. Nevertheless, there still exists residual roughness with associated debris to show that neither of the two coating processes achieves optimal smoothness. These results underscore the necessity for additional refinement of the coating techniques to improve surface uniformity.

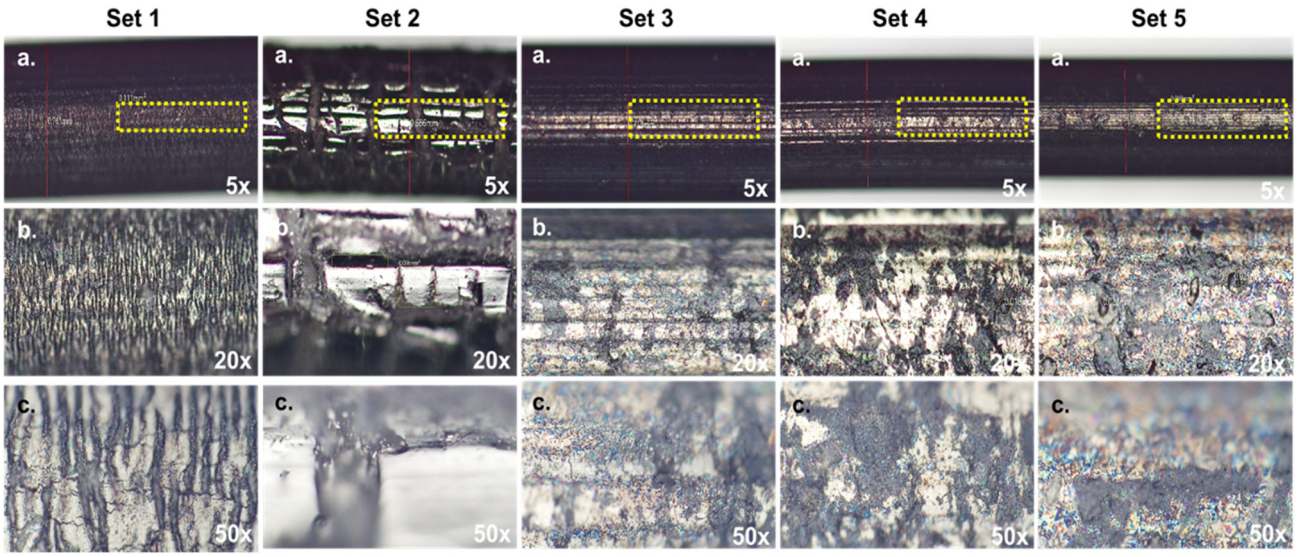


**Figure 2.** HPM images of Ni-Tn-Sn coated fibers classified into five sets as stated above. For each set, (**a**–**c**) denote the optical microscopic image at 5×, 20×, and 50× magnification.

### 3.2. Field Emission Scanning Electron Microscope (FESEM)

Field Emission Scanning Electron Microscopy (FESEM) was employed to analyze the surface morphology of the Ni-Ti-Sn coated fibers. The surface roughness and particle distribution will be emphasized in the present analysis. The FESEM images shown in Figure 3a are for the Set 1 coated fiber. The micrograph shows a fiber surface, which is significantly clean, with few impurities, which indicates a smooth coating. On the other hand, the FESEM image of Set 2 (Figure 3b) shows a slightly rougher surface with checkered film, indicating an unevenness in the deposition. This could be due to the uneven dispersion of the Ni-Ti-Sn blend, where a smaller concentration of Sn and higher concentration of Ni could result in an insufficient or undulatory coating.

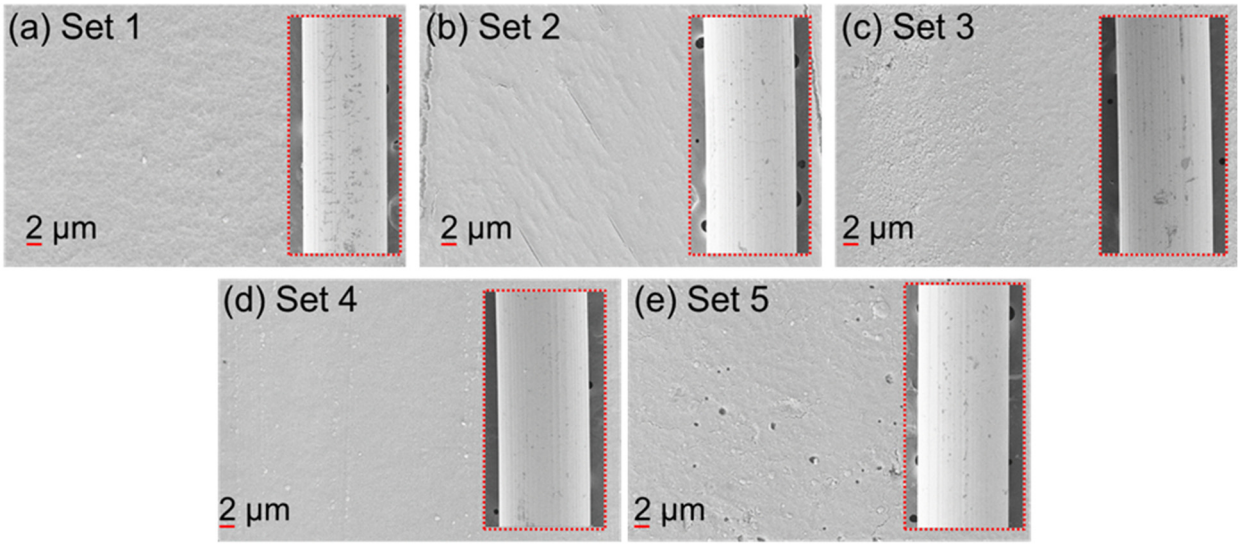


**Figure 3.** FESEM images of Ni-Ti-Sn coated fibers. (**a**–**e**) FESEM image of Set 1–Set 5, respectively. Electron microscopic image of coated fiber as insets in each figure.

The FESEM image of Set 3 (Figure 3c) indicates that the reduction in the Ni content and the increase in the Sn proportion created a surface with a coarser texture, and in some regions, a voids gap was visible. These voids appear to be related to the non-uniform nanopowder deposition on the fiber and, thus, the need for optimization in the achievement of a homogeneous coating. On the other hand, Figure 3d represents the surface morphology of Set 4, which displays a uniform, non-intermittent, and particle-isotropic distribution of Ni-Ti-Sn nanopowders across the optical fiber. The continuity of the fiber structure was confirmed by a lack of cracks and voids as well as the justified assumption of the Set 4 composition, higher in nickel and lower in tin, as being the most suitable for nanopowder deposition on optical fibers.

Nevertheless, the FESEM image for Set 5 (with the highest Ni and lowest Sn concentrations) showed unsmooth morphology with visible voids and cracks. These data reveal that the Set 5 composition is unsuitable for producing a nanocomposite coating. If all other parameters are similar to Set 4, (in the most favorable scenario), shorter bonding times of only one and two days should be enough. The results suggest that Set 4 appears to be the best option, and it can be the alternative that leads to not only to the decrease in energy consumption but also to the permanent surveillance of developed composites. Optimization of the Ni-Ti-Sn ratios is crucial for improving coating uniformity and surface quality on optical fibers. The insets shown in Figure 3a–e denote the elongated coated fiber observed under FESEM.

### 3.3. Fourier Transform Infrared Spectroscopy Analysis

Ni-Ti-Sn-coated fibers were analyzed using Fourier Transform Infrared (FTIR) spectroscopy to determine the intensity of each entity in different compositions of coated fibers.

Figure 4 shows the FTIR spectra consisting of six spectra including the uncoated fibers and the coated fibers from Set 1 to Set 5. A significant variation of peak was observed at 850 $cm^{-1}$, indicating the changes in the amount of Ni in each sample. As the amount of Ni relatively increases from Set 1 to Set 5, the peak observed conversely showed reduced peak height at the same wavelength [28]. No peak was observed at 850 $cm^{-1}$ for the uncoated fiber, which validates the presence of Ni in the coated fibers. The change in the amount of Sn in the coated fiber samples was observed at 1161 $cm^{-1}$ and 1392 $cm^{-1}$ [29,30]. Like the trend shown by Ni, Sn denotes a lower intensity in the transmittance as the amount of Sn increases from Set 1 to Set 5. According to the literature, a broadened peak observed at 2955 $cm^{-1}$ denotes the presence of Ti in the coated fibers. Since the Ti composition is the same in all the sets, an insignificant change in the peak height is notable at 2955 $cm^{-1}$ [31,32]. The FTIR spectra of the uncoated fiber shows a broadened peak at 1750 $cm^{-1}$, 1595 $cm^{-1}$, and 636 $cm^{-1}$ indicating the presence of other elements in the uncoated optical fiber. The uncoated optical fiber may include polyamide functional groups such as N-H (3200–3500 $cm^{-1}$), C=O (1640–1690 $cm^{-1}$), and C-N (1180–1360 $cm^{-1}$) bonds. Peaks at 2800–3000 $cm^{-1}$ imply aliphatic C-H stretching, whereas smaller peaks (600–1200 $cm^{-1}$) indicate bond bending or stretching. These characteristics match the polyamide backbone perhaps with additions or contaminants. The spectrum shows amide and hydrocarbon chains in polyamide.

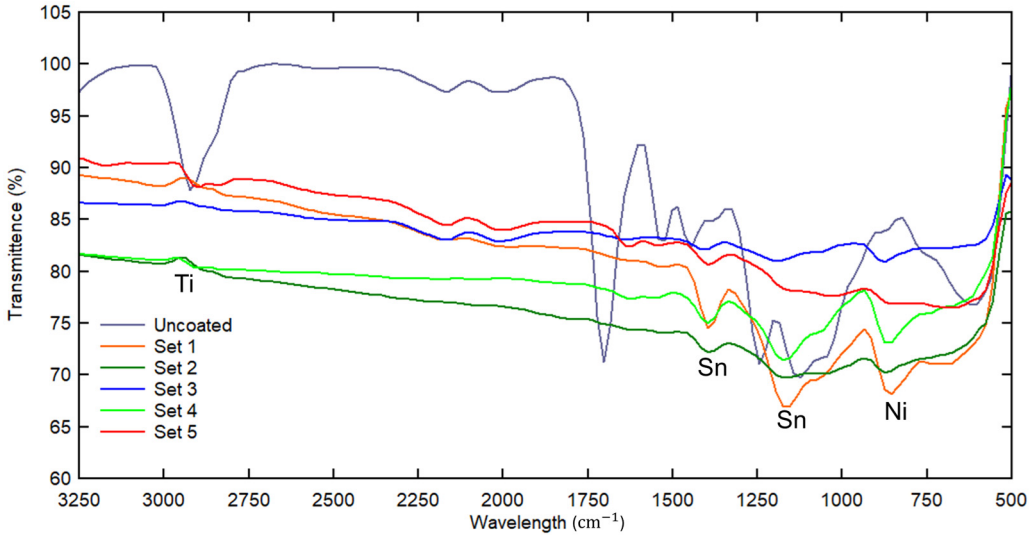


**Figure 4.** FTIR spectra consisting of uncoated and coated fibers with varying compositions of Ni-Ti-Sn.

### *3.4. Mechanical Strength*

Figure 5a depicts the overall force exerted by the nanopowder-coated fibers at various strains, while Figure 5b shows the tensile strength and elongation of the composite at varying alloy compositions. From Figure 5b, it was seen that Set 5 exhibited the highest tensile strength of 28 MPa, whereas the minimum tensile strength was obtained for Set 2 (26.2 MPa). Similarly, the maximum elongation at fracture was achieved by Set 5 (7.1%), whereas Set 1 had the minimum elongation of 5.1% (Figure 5c). It is evident from the findings above that the mechanical properties of the alloy coating are solely responsible for the strength of the polymer fibers. Composites with higher tin content showed the highest tensile strength and percent elongation, hence depicting better mechanical properties. The coated fiber was compared with an uncoated fiber where the uncoated fiber had a tensile strength of 29.6 MPa with an elongation of 5.9%. Set 1 had a tensile strength similar to uncoated fiber (29.6 MPa), while the tensile strength of Set 4 was 29.4 MPa with varying elongations. This indicates that Set 4 had an increased ductility with an elongation of 6.3%.

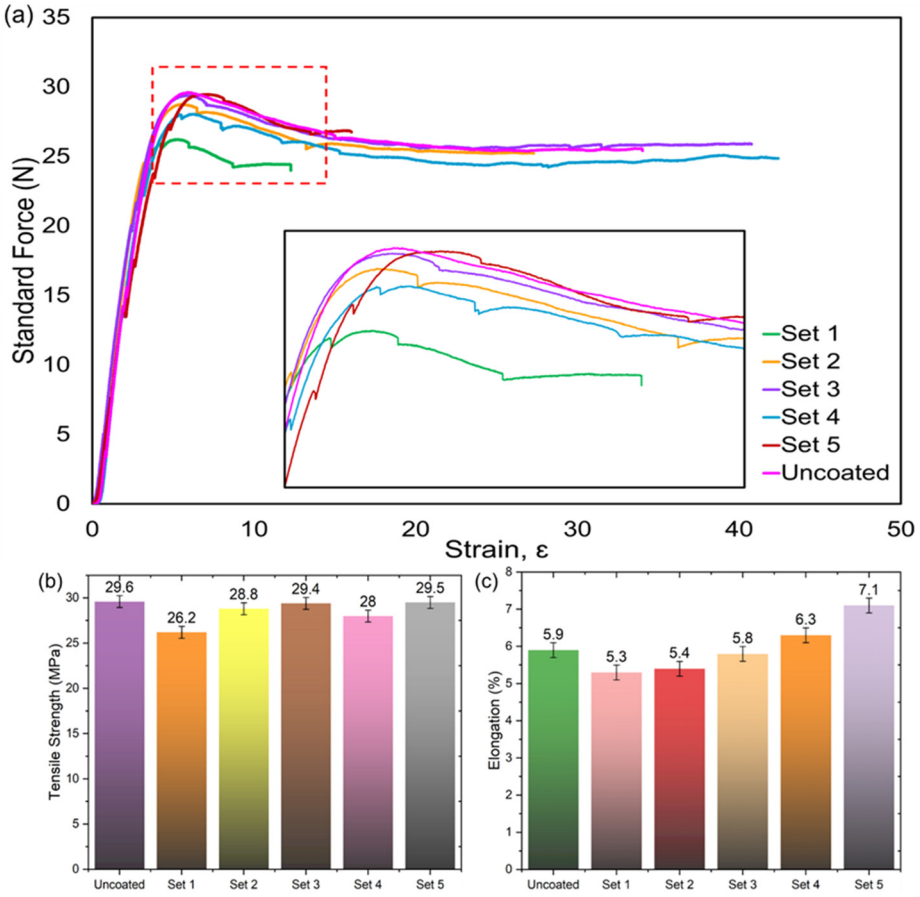


**Figure 5.** (**a**) Trend of force exerted by optical fiber over a range of applied strains; (**b**) tensile strength and (**c**) elongation of the optical fiber coated with Ni-Ti-Sn nanopowders.

On the other hand, Set 2 showed a decrease in tensile strength (26.2 MPa), which indicates structural compromise, although its elongation was slightly higher at 5.4%. Therefore, Set 2 might not be suitable for applications requiring high tensile integrity. Set 3 recorded a minimal reduction in tensile strength of 28.8 MPa with a percentage elongation increase by 5.8% indicating an equilibrious modification. Set 5 a exhibited significant increase in elongation (7.1%), although at the expense of lower tensile strength of 28.0 MPa, which indicates that the coating composition significantly enhances flexibility. Hence, Set 5 can be used for applications where flexibility is desirable at the cost of tensile strength, since it has a profound increase in ductility.

The tensile test results show the different influences of alloy coating on the mechanical properties of polymer fibers. To this end, Set 4 has provided the best equilibrium in offering increased ductility with minimum compromise on tensile strength. Since it offers an optimum balance between strength and flexibility; the composition will be suitable for applications related to moderate tensile performance with improved ductility. With such a drastic loss in tensile strength, Set 2 would have limited use under high-stress applications, while Set 5, with its exceptionally high ductility, would be highly suitable for applications that require very high ductility. To this end, the authors suggest that the selection of alloy coating needs to be based on specific mechanical requirements for the intended application and, as such, needs to be balanced between tensile strength and elongation.

### *3.5. Thermogravimetric Analysis (TGA)*

One or more distinct regions present in the TGA curve corresponds to different thermal events. Initial mass loss occurs at lower temperatures, where water or some other volatile components may be present in the sample and can evaporate and cause an initial mass loss, which is characterized by a gradual fall in mass recorded on the TGA

curve. The main decomposition occurs when a further increase in temperature results in decomposition of the coating material. The temperature of onset, rate of decomposition, and extent of mass loss reflect thermal stability and kinetics for the decomposition of the coating [33]. Residue formation is the stage beyond the main decomposition region; some materials may leave behind a residue due to incomplete decomposition or the presence of inert components. The residual mass and composition can offer insights into the thermal decomposition products and the presence of alloying elements in the coating. Asim et al. [34] used silane coating on natural fiber with synthetic phenolic resin to achieve remarkable thermal stability and 20–35 wt % char residue at 700 °C. Two thermal stability phases were observed: 250–350 °C for kenaf fiber and PALF degradation and 300–500 °C for phenolic resin degradation. Similarly, the thermal behavior of $KMnO_4$-treated plantain fiber-reinforced epoxy composites (0.025%, 0.05%, and 0.10%) was studied by Imoisili [34]. The TGA results indicate that the cellulose manganite complex has been linked to the thermal stability of KMnO4 treated with 0.025% and 0.05% fibers. The proposed coated synthetic fibers possess better thermal stability of 550 °C and 700 °C, which is comparatively higher than natural fiber-coated samples.

Figure 6a depicts the TGA graph for the experimental sets. The first weight loss region occurs between 200 and 500 °C with a weight of 0.01 mg. The second weight loss region occurs between 550 and 700 °C. This weight loss is caused by the decomposition reaction of the nanopowders. The uncoated fiber shows a minor mass loss of 0.50%, suggesting high thermal stability with minimal degradation. Set 1 exhibits a small increase in mass (0.57%), which could be attributed to experimental errors such as contamination or oxidation. Set 2 and Set 3 show minor mass losses of 1.41% and 0.02%, respectively, indicating good thermal stability with minimal degradation. Set 4 demonstrates a moderate mass loss of 2.05%, pointing to some degradation or volatilization of the coating. Set 5 showed a significant mass loss of −12.84%, indicating substantial degradation or a high volatile content in the coating, which suggests that this coating might not be thermally stable compared to the other compositions.

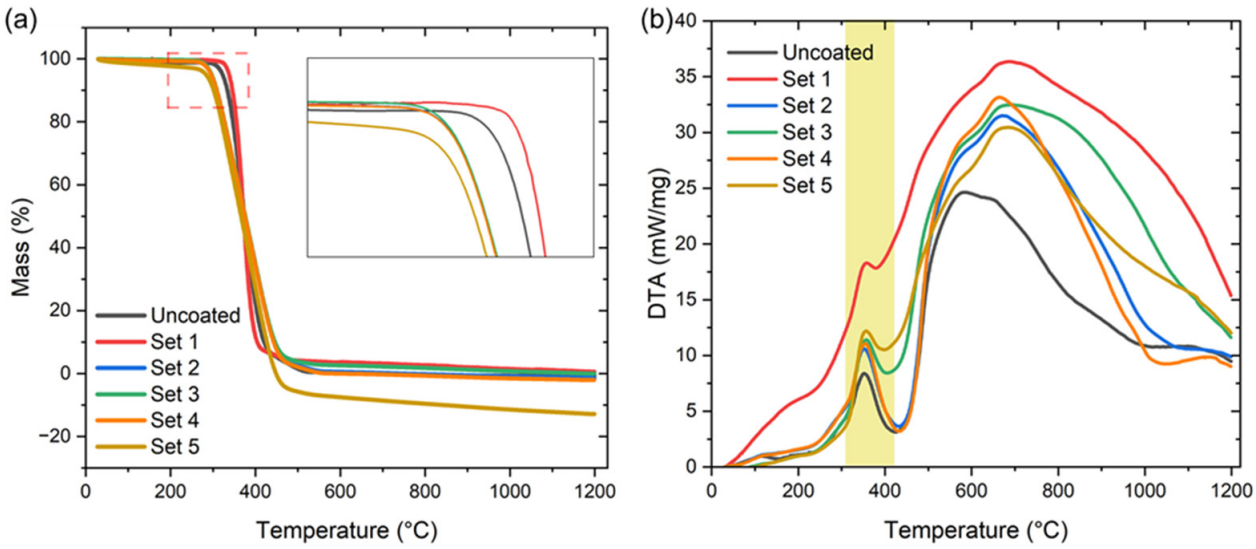


**Figure 6.** (**a**) Thermal analysis of Ni-Ti-Sn coated fibers evaluated through (**a**) thermogravimetric analysis and (**b**) differential thermal analysis.

### *3.6. Differential Thermal Analysis (DTA)*

Figure 6b shows the DTA plots of coated fibers and uncoated baseline. The uncoated fiber had a melting point of 425.0 °C, which was used as the reference. Set 1 had a considerably lower melting point of 379.5 °C, indicating this coating lowers the thermal stability of the fiber. In contrast, the melting points for Set 2 and Set 4 were significantly higher at 431.7 °C and 433.4 °C, respectively, suggesting increased thermal stability compared to the

uncoated sample. Set 3 showed a melting point of 404.1 °C, which was moderately high and considered a slight improvement in stability, although it was not as significant as Set 2 and Set 4. Set 5 shows greater weight loss compared to the uncoated sample due to the presence of volatile compounds, reactive additives, or less thermally stable materials. Usually, metal alloys do not completely decompose at 400 °C; instead, they may undergo oxidation or phase transformations. In our results, the significant weight loss at this temperature can be attributed to the non-metallic components of coatings.

Although Set 5 exhibited high mass loss from TGA, the high melting point at 397.6 °C showed that the composite was (moderately) thermally stable, although it was compromised by the coating instability. More importantly, DTA results showed the correlation of noticeable thermal transitions with mechanical integrity for the alloy coatings. For instance, Sets 2 and 4 had higher melting points; hence, their enhanced thermal stability allowed the composite to be relatively more viable compared to Set 1, which exhibited a lower melting point with significant mass loss (reduced thermal resistance). Despite high flexibility, Set 5 exhibited a lower melting point and higher mass loss in TGA. The DTA and TGA data provided the complete thermal behavior of the nanopowder-coated fibers. Coatings of Set 2 and Set 4 have better thermal stability, and as such, such coatings will be deemed suitable for applications that require improved heat resistance as opposed to coatings of Set 1, where the action of thermal stresses results in lower melting points and instability.

### *3.7. Fractured Fibers—Microscopic Vision*

The surface morphology of fractured Ni-Ti-Sn nanopowder-coated fibers was examined using FESEM to analyze the failure characteristics post-fracture. These images provide detailed insights into surface defects, particle detachment, and coating integrity at the fracture sites. Figure 7a(i) shows the cross-sectional FESEM image of the fractured Set 1 fiber, while Figure 7a(ii) reveals pronounced surface roughness and severe cracks at the fracture zone. Particle detachment is evident along the fiber surface, indicating that the Ni-Ti-Sn composition in Set 1 lacks sufficient durability to withstand mechanical stress, particularly under harsh conditions. The severity of the observed cracks suggests the composition is unsuitable for applications requiring high structural integrity.

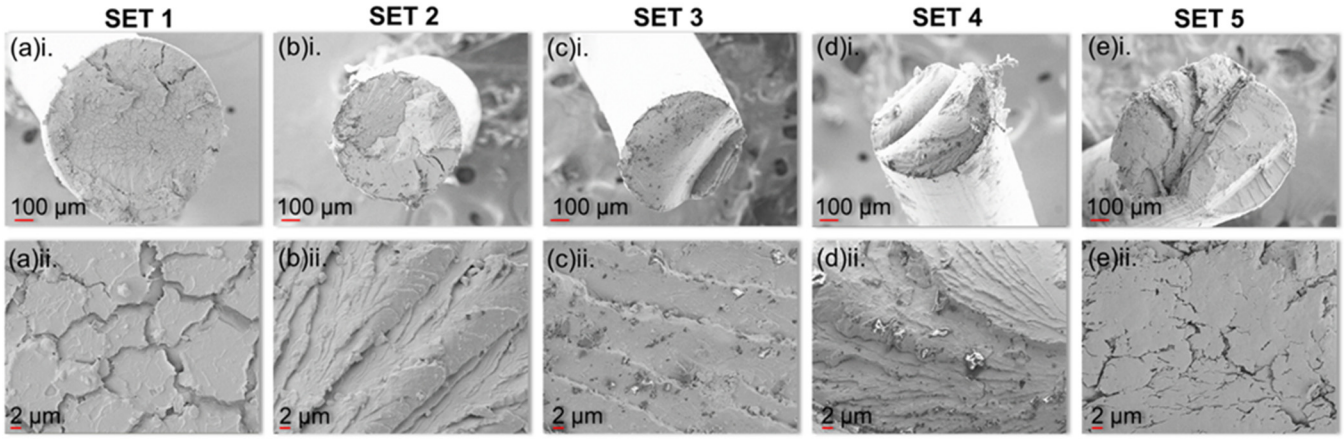


**Figure 7.** FESEM images of fractured fibers coated with varying compositions of Ni-Ti-Sn. (**a**–**e**) denotes Set 1–Set 5; where part (**i**) and (**ii**) reveal the electron microscopic view of the cross-sectional fiber and surface region, respectively.

Figure 7b(i) shows the cross-sectional region of Set 2 fibers, while Figure 7b(ii) shows a rough yet less severely cracked surface compared to Set 1. The reduced fracture severity suggests that increasing the amount of Ni and reducing Sn improves the coating's mechanical durability. The tightly packed structure of these layers in Set 2 lacks the gap through which it can easily rupture by applying a load.

Figure 7c(i) shows the cross-sectional image of Set 3 where fewer voids and cracks on the surface morphology were seen, indicating enhanced adhesion between the Ni-Ti-Sn film and the substrate's medium. Therefore, the composition of Set 3 ascertains enhanced coating adhesion and fracture resistance compared to previous sets. Figure 7d shows that the fractured surface was damaged, rough and uneven with the visible presence of voids, all of which can be caused by the detachment of the particles under mechanical stress. This indicates that the composition of Set 4 did not provide enough hardness for the composite. Figure 7e shows the SEM images of Set 5 where the fracture pattern noticed a minor void presence and a few cracks. In addition, the surface was more rigid compared to other surfaces, which indicates that Set 5 hardened during the coating process. The increased hardness likely promotes adhesion and enhanced the strength of the whole structure, all of which indicates that Set 5 has better fracture resistance compared to the other compositions.

## 4. Conclusions

The present study comprehensively studied the mechanical and thermal properties of alloy-coated polymer fibers. The metallurgical microscopic characterizations showed that the coatings were well dispersed within the coated layer, and Set 5 (48.8% Ni, 50.2% Ti, and 1% Sn) exhibited the most even surface among other compositions. Mechanical testing showed that Set 5 had a tensile strength of 29.5 MPa, which was quite similar to that of an uncoated fiber at 29.6 MPa although with increased elongation at fracture by 25%. The uniform thickness of the coating of 0.50 μm and SEM imaging verified the accurate deposition process that contributed toward improved mechanical performance. Coated fibers subjected to load exhibited low level of stress and deformation compared to uncoated samples, hence ascertaining that coating treatment enhanced mechanical integrity. To this end, alloy-coated fibers with superior thermal stability, mechanical strength, and optical clarity hold great potential in applications related to fiber optics and structural health monitoring among other advanced engineering areas. The results obtained from the present study allow further possibilities of research into coating techniques, long-term durability, and material optimization strategies.

**Author Contributions:** Conceptualization, Methodology, E.N., G.F. and C.K.A.; Software, S.M.S., K.M. and S.R., Validation, E.N., N.D. and A.C.; Resources, G.F.; Data curation, E.N. and A.C.; Writing—original draft, S.M.S., A.C. and K.M.; Writing—review and editing, K.M., G.F., C.K.A. and S.R; Supervision, C.K.A.; Project administration, E.N., N.D. and G.F.; Funding acquisition, G.F. All authors have read and agreed to the published version of the manuscript.

**Funding:** This research received no external funding.

**Data Availability Statement:** The data presented in this study are available within the article.

**Conflicts of Interest:** The authors declare that they have no known competing financial interests or personal relationships that could have appeared to influence the work reported in this paper.

## References

1. Ngiejungbwen, L.A.; Hamdaoui, H.; Chen, M.Y. Polymer Optical Fiber and Fiber Bragg Grating Sensors for Biomedical Engineering Applications: A Comprehensive Review. *Opt. Laser Technol.* **2024**, *170*, 110187. [CrossRef]
2. Wang, L.; Kelly, P.V.; Ozveren, N.; Zhang, X.; Korey, M.; Chen, C.; Li, K.; Bhandari, S.; Tekinalp, H.; Zhao, X.; et al. Multifunctional Polymer Composite Coatings and Adhesives by Incorporating Cellulose Nanomaterials. *Matter* **2023**, *6*, 344–372. [CrossRef]
3. Rahman, M.; Ordu, M. Long-Length 3D Printed Hollow-Core Polymer Optical Fiber for Wideband Light Guidance. *Opt. Fiber Technol.* **2023**, *81*, 103512. [CrossRef]
4. Jing, W.; Feng, L.; Wang, B.; Zhang, W.; Xu, K.; Al Aboody, M.S.; Mickymaray, S.; Peng, K. Polymer-Ceramic Fiber Nanocomposite Coatings on Titanium Metal Implant Devices for Diseased Bone Tissue Regeneration. *J. Sci. Adv. Mater. Devices* **2021**, *6*, 399–406. [CrossRef]
5. Alemour, B.; Badran, O.; Hassan, M.R. A Review of Using Conductive Composite Materials in Solving Lightening Strike and Ice Accumulation Problems in Aviation. *J. Aerosp. Technol. Manag.* **2019**, *11*, e1919. [CrossRef]
6. Zhang, Z.; Huang, Y.; Xie, Q.; Liu, G.; Ma, C.; Zhang, G. Functional Polymer–Ceramic Hybrid Coatings: Status, Progress, and Trend. *Prog. Polym. Sci.* **2024**, *154*, 101840. [CrossRef]

7. Ayesta, I.; Azkune, M.; Illarramendi, M.A.; Arrospide, E.; Zubia, J.; Durana, G. Fabrication and Characterization of Active Polymer Optical Fibers with a Ring-Doped Structure. *Opt. Fiber Technol.* **2023**, *75*, 103209. [CrossRef]
8. Mohammed, P.A.; Abdulla, R.M.; Aziz, S.B. Light-Matter Interaction during and Post Polymerization in Self-Written Polymer Waveguide Integrated with Optical Fibers. *Phys. B Condens. Matter* **2024**, *695*, 416481. [CrossRef]
9. Sandhanshiv, R.D.; Patel, D.M. Carbon Fibre Reinforced Composite Material: Review of Properties and Processing for Various Metal Matrix Materials. *IOP Conf. Ser. Mater. Sci. Eng.* **2019**, *810*, 0120140. [CrossRef]
10. Sun, J.; Yamanaka, K.; Zhou, S.; Saito, H.; Ichikawa, Y.; Ogawa, K.; Chiba, A. Dynamic Recrystallization of Sn Coatings on Carbon-Fiber-Reinforced Plastics during Cold Spray Additive Manufacturing. *Addit. Manuf.* **2022**, *56*, 102949. [CrossRef]
11. Liu, S.; Feng, K.; Xu, W.; Shi, X.; Xu, Z.; Wang, C. Metal-Organic Framework Tin Doped Nickel Phosphide/Carbon Composites for High Performance Sodium Ion Batteries. *J. Energy Storage* **2023**, *74*, 109517. [CrossRef]
12. Nazrin, K.; Nagashree, M.C.; Srivathsa, M.; Rajendra, B.V. Tuning of Structure, Surface Morphology and Optical Properties of Spray-Coated Nickel Tin Oxide Thin Films by Heat Treatment. *Phys. B Condens. Matter* **2024**, *691*, 416382. [CrossRef]
13. Davoodi, F.; Ashrafizadeh, F.; Atapour, M.; Akbari-Kharaji, E.; Mokhtari, R. Anticorrosion Performance of TiN Coating with Electroless Nickel-Phosphorus Interlayer on Al 6061 Alloy. *Mater. Chem. Phys.* **2023**, *296*, 127170. [CrossRef]
14. Isotahdon, E.; Huttunen-Saarivirta, E.; Kuokkala, V.T.; Paju, M.; Frisk, L. Corrosion Protection Provided by Electrolytic Nickel and Tin Coatings for Nd-Fe-B Magnets. *J. Alloys Compd.* **2014**, *585*, 203–213. [CrossRef]
15. Sun, J.; Yamanaka, K.; Zhou, S.; Saito, H.; Ichikawa, Y.; Ogawa, K.; Chiba, A. Adhesion Mechanism of Cold-Sprayed Sn Coatings on Carbon Fiber Reinforced Plastics. *Appl. Surf. Sci.* **2022**, *579*, 151873. [CrossRef]
16. Akhtar, K.; Khan, S.B.; Bakhsh, E.M.; Asiri, A.M. A Nanocomposite of Nickel Oxide-Tin Oxide and Carboxymethylcellulose Coated Cotton Fibres for Catalytic Reduction of Water Pollutants. *J. Mol. Liq.* **2023**, *375*, 121275. [CrossRef]
17. Mishra, S.K.; Rani, S.; Gupta, B.D. Surface Plasmon Resonance Based Fiber Optic Hydrogen Sulphide Gas Sensor Utilizing Nickel Oxide Doped ITO Thin Film. *Sens. Actuators B Chem.* **2014**, *195*, 215–222. [CrossRef]
18. Magdy, M.A.M.; Kooli, F.; Alamri, S.N. Electrodeposition and Characterization of Nickel-TiN Microcomposite Coatings. *Int. J. Electrochem. Sci.* **2013**, *8*, 12308–12320.
19. Wierzbicka, E.; Vaghefinazari, B.; Lamaka, S.V.; Zheludkevich, M.L.; Mohedano, M.; Moreno, L.; Visser, P.; Rodriguez, A.; Velasco, J.; Arrabal, R.; et al. Flash-PEO as an Alternative to Chromate Conversion Coatings for Corrosion Protection of Mg Alloy. *Corros. Sci.* **2021**, *180*, 109189. [CrossRef]
20. Amiri, L.; Narjis, A.; Nkhaili, L.; Bousseta, M.; Elmassi, S.; Tchenka, A.; Drissi, S.; Abali, A.; Somaily, H.H.; El Kissani, A.; et al. Spectroscopic Study and Thermoelectric Properties of Copper Sulfide Thin Films Prepared by the Flash Evaporation Method. *J. Alloys Compd.* **2022**, *924*, 166479. [CrossRef]
21. Sekar, R.; Shivananju, B.N.; Lakshmi, K.P.; Asokan, S. Dual Functional Performance of Fiber Bragg Gratings Coated with Metals Using Flash Evaporation Technique. *Opt. Fiber Technol.* **2012**, *18*, 183–185. [CrossRef]
22. Li, B.; Zhang, L.; Yan, T.; Fu, H.; Zhang, H.; Li, H.; Zhang, H. Mechanical properties of the (Ti0.615Zr0.385)100-3.9(Cu2.3Fe1.6) alloys containing amorphous martensite. *J. Alloys Compd.* **2023**, *958*, 170511. [CrossRef]
23. Yang, G.; Zhou, L.; Wang, M.; Xiang, T.; Pan, D.; Zhu, J.; Su, F.; Ji, Y.; Liu, C.; Shen, C. Polymer composites designed with 3D fibrous CNT "tracks" achieving excellent thermal conductivity and electromagnetic interference shielding efficiency. *Nano Res.* **2023**, *16*, 11411–11421. [CrossRef]
24. Lee, S.H.; Yu, S.; Shahzad, F.; Hong, J.P.; Kim, W.N.; Park, C.; Hong, S.M.; Koo, C.M. Highly anisotropic Cu oblate ellipsoids incorporated polymer composites with excellent performance for broadband electromagnetic interference shielding. *Compos. Sci. Technol.* **2017**, *144*, 57–62. [CrossRef]
25. Sun, R.; Zhang, H.; Liu, J.; Xie, X.; Yang, R.; Li, Y.; Hong, S.; Yu, Z. Highly Conductive Transition Metal Carbide/Carbonitride (MXene)@polystyrene Nanocomposites Fabricated by Electrostatic Assembly for Highly Efficient Electromagnetic Interference Shielding. *Adv. Funct. Mater.* **2017**, *27*, 1702807. [CrossRef]
26. Soni, A.; Das, P.K.; Gupta, S.K.; Saha, A.; Rajendran, S.; Kamyab, H.; Yusuf, M. An Overview of Recent Trends and Future Prospects of Sustainable Natural Fiber-Reinforced Polymeric Composites for Tribological Applications. *Ind. Crops Prod.* **2024**, *222*, 119501. [CrossRef]
27. Soni, S.K.; Thomas, B.; Thomas, S.B.; Tile, P.S.; Sakharwade, S.G. Carbon Nanotubes as Exceptional Nanofillers in Polymer and Polymer/Fiber Nanocomposites: An Extensive Review. *Mater. Today Commun.* **2023**, *37*, 107358. [CrossRef]
28. Sudhasree, S.; Shakila Banu, A.; Brindha, P.; Kurian, G.A. Synthesis of Nickel Nanoparticles by Chemical and Green Route and Their Comparison in Respect to Biological Effect and Toxicity. *Toxicol. Environ. Chem.* **2014**, *96*, 743–754. [CrossRef]
29. Petrov, T.; Markova, I.; Chauvet, O. Sem and FTIR Spectroscopy Study of Cu, Sn and Cu-Sn Nanoparticles. *J. Univ. Chem. Technol. Metall.* **2012**, *47*, 197–206.
30. Thirumoorthi, M.; Thomas Joseph Prakash, J. Structure, Optical and Electrical Properties of Indium Tin Oxide Ultra Thin Films Prepared by Jet Nebulizer Spray Pyrolysis Technique. *J. Asian Ceram. Soc.* **2016**, *4*, 124–132. [CrossRef]
31. Idris, A.; Majidnia, Z.; Nor Kamarudin, K.S. Photocatalyst Treatment for Lead(II) Using Titanium Oxide Nanoparticles Embedded in PVA-Alginate Beads. *Desalination Water Treat* **2016**, *57*, 5035–5044. [CrossRef]
32. Tarafdar, A.; Raliya, R.; Wang, W.-N.; Biswas, P.; Tarafdar, J.C. Green synthesis of $TiO_2$ nanoparticle using Aspergillus tubingensis. *Adv. Sci. Eng. Med.* **2013**, *5*, 943–949. [CrossRef]

33. Asim, M.; Paridah, M.T.; Saba, N.; Jawaid, M.; Alothman, O.Y.; Nasir, M.; Almutairi, Z. Thermal, physical properties and flammability of silane treated kenaf/pineapple leaf fibres phenolic hybrid composites. *Compos. Struct.* **2018**, *202*, 1330–1338. [CrossRef]
34. Imoisili, P.E.; Jen, T. Mechanical and water absorption behaviour of potassium permanganate ($KMnO_4$) treated plantain (Musa Paradisiacal) fibre/epoxy bio-composites. *J. Mater. Res. Technol.* **2020**, *9*, 8705–8713. [CrossRef]